Detection Of Unbalance MMF In Permanent Magnet Direct Current Machines Using Vibration

Osman Gergöz
Faz Elektrik Motor Makina San ve Tic. A. S.,
PK. 104 35150 Bornova-Izmir,Turkey

Eyüp Akpinar
Department of Electrical and Electronics Engineering
Dokuz Eylül University
35160 Buca-Izmir,Turkey

Abstract **The frequency spectrum of vibration produced in electric motors has been recently used for improving the detection of motor failures during the assembling process. In this work, the vibration test has been done on permanent magnet direct current motor (PMDCM) used in wheelchair to identify if the permanent magnet poles have the exact dimensions and positions around the periphery of stator core. The electromagnetic radial force and vibration developed by the magnets are predicted by computer analysis and compared to the experimental results.**

Index Terms-**Electrical machines, vibration, noise**

I. INTRODUCTION

The electromagnetic radial forces, known as Maxwell forces are derived in [1] as a function of field distributed in the air gap. The harmonics in the air gap field of a PMDCM are produced due to variation of air gap between the stator and rotor, even if, the armature current is not circulating. In the permanent magnet direct current motors, shown in figure 1, the shape of permanent magnet affects the harmonics of the air gap field.

The permeance in the air gap is inversely proportional to the air gap length between the stator and rotor [2]. The slotting structure of the rotor produces fluctuating permeance distribution in the gap. The MMF produced by magnets in two pole machine has same magnitude but, in the opposite direction. The multiplication of the permeance and MMF distribution gives flux distribution in the air gap. The electromagnetic radial force per area can be computed from the square of the flux density. The harmonic components of the electromagnetic radial force, providing the spectrum of vibration [3, 5], are computed by using fast-fourier transform.

A modified magnetic circuit method has been applied in this work for the analysis of the PMDCM with differing armature, magnet and yoke lengths including non-linear material behavior of steel and permanent magnet [4].

The finite-element and finite-difference methods are usually used for finding the flux density distribution in a machine including the effect of slot skewing and saturation. Although the analytical solution of the magnetic field provides an approximate flux density distribution in the magnetic circuit, it is time-saving technique and sufficiently accurate to use in estimating the frequency components, not their amplitudes, of forces and resulting vibration and noise of the motor [6]. The mechanical damping of the material is kept out of scope of this paper.

II. ANALYSIS OF MAGNETIC CIRCUIT

The MMF created by the permanent magnets can be specified due to the sum of MMF drops on each part, i.e., the yoke (stator back core), air gap, teeth and rotor core.

In the analysis of magnetic circuit, the accurate prediction of flux distribution can be carried out by considering the non-linear shape of magnetization characteristics.

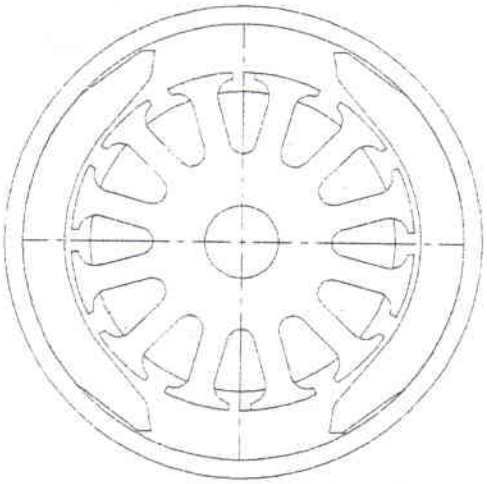

Figure1. Structure of permanent magnet dc motor

The demagnetisation curve of the ferrite magnet shown in figure 2 is represented by the relation given in (1);

$$H(B) = \frac{H_c}{B_r} B - H_c \qquad (1)$$

where $H_c = 295 \times 10^3$ and $B_r = 0.391$

If the effect of magnet overhang is considered, the demagnetization characteristic of magnet can be modified by changing flux density value by a factor for a given magnetic strength and considering the length of magnet same as armature. An empirical relation for this

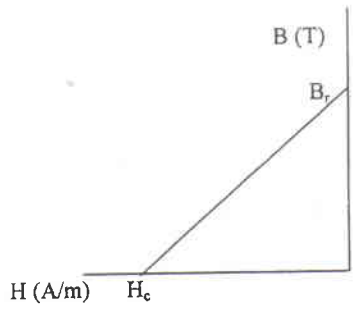

Figure 2. Demagnetisation curve of a magnet

modification is given in [4, 7]. The length of magnet and armature of PMDCM used here is same, therefore, the modification is not needed. The MMF created by the magnet given in (2) is obtained from (1) in terms of operating flux and machine dimensions defined in table 1.

$$F_m = \frac{H_c}{B_r}\frac{L_m}{S_m}\Phi - L_m H_c \qquad (2)$$

where

$$L_m = (D_i - D_m)/2 \quad \text{and} \quad S_m = \alpha\pi D_m l_m/360$$

The magnetisation characteristic of steel used for yoke is given in Figure 3. This characteristic has been interpolated by two curves. The first curve, which is third order (non-linear) given in (3), is considered from zero to knee point (B_k, H_k). The second one, that is the linear one given in (4), is from the knee point to the end (B_e, H_e). The knee point (B_k, H_k) and end point (B_e, H_e) of the magnetisation characteristic are selected on the curve as (1.63 T, 4 kA/m) and (2 T, 16 kA/m) respectively.

$$H(B)_{s1} = a_0 + a_1 B + a_2 B^2 + a_3 B^3 \qquad (3)$$

$$H(B)_{s2} = \frac{H_e - H_k}{(B_e - B_k)}(B - B_k) + H_k \qquad (4)$$

where a_0, a_1, a_2, and a_3 are the interpolating coefficients.

$$a_0 = 0.0051,\ a_1 = 1.421,\ a_2 = -1.447,\ a_3 = 0.416$$

The magnetisation characteristic of yoke's steel is modified by multiplying flux density B by a factor, K_s which is the ratio of yoke length l_y to armature length for each flux intensity H value [4].

$$K_s = l_y/l_{ar} \qquad (5)$$

The modified F-Φ curve of yoke's steel for the non-linear (6) and linear (7) regions are obtained from (3) and (4) respectively;

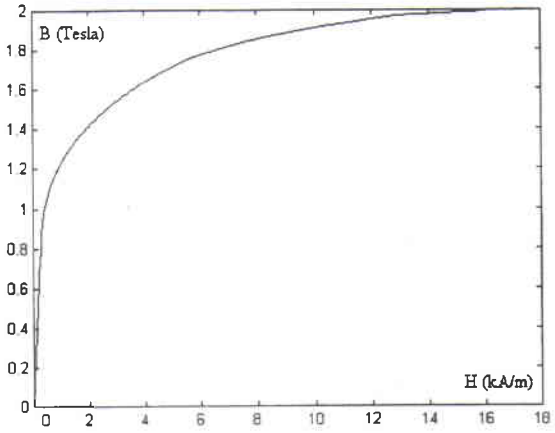

Figure 3. The magnetisation characteristic of steel used in yoke

$$F_{y1} = \left(a_0 L_y + a_1 \frac{L_y}{S_y}\Phi + a_2 \frac{L_y}{S_y^2}\Phi^2 + a_3 \frac{L_y}{S_y^3}\Phi^3\right) 10^3 \qquad (6)$$

$$F_{y2} = L_y \frac{H_e - H_k}{K_s(B_e - B_k)}\left(\frac{l}{S_y}\Phi - K_s B_k\right) + L_y H_k \qquad (7)$$

where

$$L_y = \pi(D_o + D_i)/4 \quad , \quad S_y = l_y(D_o - D_i)/2$$

The MMF drop on the air gap is computed by using the equation (8);

$$F_a = \frac{L_a}{\mu_0 S_m}\Phi \qquad (8)$$

where

$$L_a = D_m - D_a$$

The teeth MMF drop is small compared to the air gap and yoke MMF drops, therefore, it has been neglected. The operating point of motor is determined at

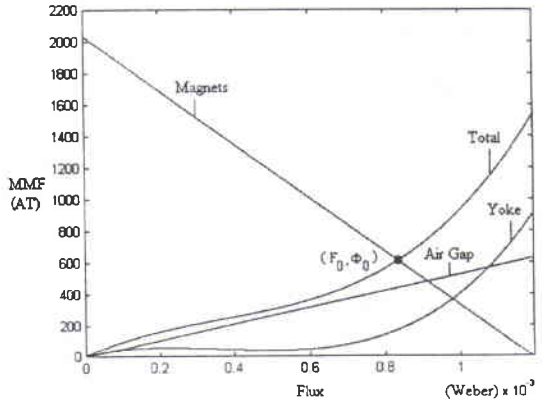

Figure 4. The modified MMF-Φ curves using the interpolation coefficients

the intersection point of total MMF drop and MMF produced by magnet under no-load condition. Hence,

$$F_m = F_{yl} + F_a \qquad (9)$$

The solution of equation (9) is the operating point (F_o, Φ_o) as shown on figure 4.

$\Phi_0 = 82.8 \times 10^{-5}$ Weber and $F_0 = 600$ AT

III. MOTOR DIMENSIONS

A cross section view of 24 volts, 360 watts motor having equal lengths of armature and magnets is given in figure 1. The stator back core is a round steel that has two permanent magnets stuck to its inner side. The armature has 12 semi-closed slots. Two test motors have been used in this analysis. The dimensions of these motors given in Table 1 are identical. The occupation of permanent magnet in one of them is 150 degrees (central angle) around the periphery of stator core, as that of the other is 120 degrees.

Table 1 The dimensions of the PMDCM.

Yoke outer diameter	D_o	78.2	mm
Yoke inner diameter	D_i	72	mm
Yoke length	l_y	101	mm
Magnet inner diameter	D_m	58.2	mm
Magnet length	l_m	50	mm
Magnet thickness	W_m	6.9	mm
Armature outer diameter	D_a	56.1	mm
Armature length	l_{ar}	50	mm
Slot width	W_s	3.4	mm
Tooth width	W_t	11	mm
Central angle of magnet	α	120 & 150	Degree

IV. ELECTROMAGNETIC RADIAL FORCES

In this paper, the permeance wave method is used to determine the flux density distribution in the air gap. The permeance waves are formulated by considering the effect of sloting. The flux density distribution in the air gap is obtained by the multiplication of the MMF and permeance waves [3]. When the boundaries are so highly permeable, it can be assumed that H is zero inside the iron boundary, a simple method formulated in (12) can be used to calculate the Maxwell's force per unit area, that acts on the stator and rotor surfaces [1, 3].

The slotting structure of the rotor and reluctance between the permanent magnets on the stator cause the fluctuating permeance distribution along the air gap, as shown in figure 5. The analysis of the permeance for semi-closed and rectangular structures of the slots can be found in [8, 9]. The analysis carried out here depends on the rectangular shape by assuming that air gap under a permanent magnet takes two different values. One of them is over the tooth l_1 and the other is over the slot l_2. The average tooth and slot angles are found to be 22.5 and 7.5 degrees respectively.

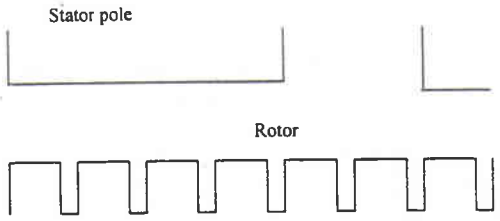

Figure 5. Structure of the permeance in the air gap

The waveshape of flux distribution is related to the central angle of the magnets. The flux density distribution also fluctuates between B_1 and B_2.

$$B_1 = \frac{F_0 \mu_0}{l_1} \qquad (10)$$

and

$$B_2 = \frac{F_0 \mu_0}{l_2} \qquad (11)$$

The electromagnetic radial force per area can be written in terms of angular position of the rotor as follows;

$$\Delta(\theta) = \frac{B^2(\theta)}{2\mu_0} \qquad (12)$$

The fast fourier transform of electromagnetic radial force distribution (12) is computed by using Matlab [10].

V. RESULTS

In order to investigate the validity of the theoretical calculation of the frequency spectrum of vibration on stator frame, an experimental work was carried out on two permanent magnet dc motors having the design data in table 1. The frequency spectrum of the vibration is obtained by a test circuit containing a PC, preamplifier, vibration sensor and data acquisition system. The vibration was measured on the stator frame. The motor was rotated by an external prime mover at 3600 rpm. A flexible coupling was used to isolate the shaft of the PMDCM from the prime mover. The end shields were removed and the carbon brushes were taken out of motor to eliminate their effect on the vibration and noise. The motor was isolated from the foundation using rubber pads.

In this work, the composition of the harmonics is identified rather than percentages. Here, l_2 is set to a value which is fourteen times of l_1. The fundamental frequency of vibration is found at the rotor speed in terms of revolution per seconds. The frequency range of the vibration measuring instrument was between 10 Hz and 1 kHz [11]. The predicted and experimental results obtained using the FFT (fast-Fourier transform) show that the 1^{st} -12^{th} (except 3^{rd} and 9^{th}) harmonic components

exist in the spectrum of vibration as shown in figure 6a and 6b.

Figure 7 shows the spectrum of vibration on test motor with 150 degrees occupation of magnets. Figure 6a and 7 present that the spectrum of vibration on the stator under no-load condition. The spectrum of vibration depends on the circumference length of permanent magnets, even if all motor dimensions are kept identical. The 6^{th} harmonic appears for both machines as the dominant slot harmonics since the rotor has six slots per pole. The 3^{rd} and 6^{th} harmonics are disappeared for the machine having 120 degrees occupation of magnets.

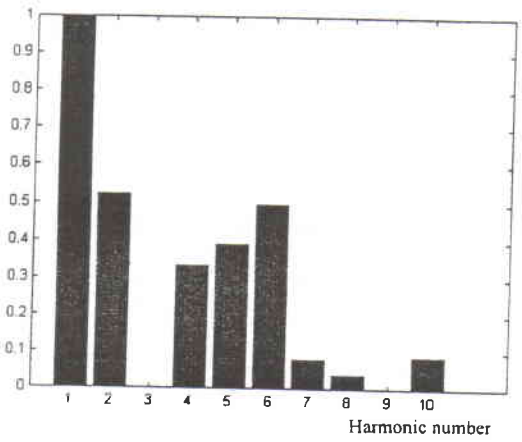

Figure 6a. Predicted spectrum of vibration on the test motor with $\alpha_1=120^0$

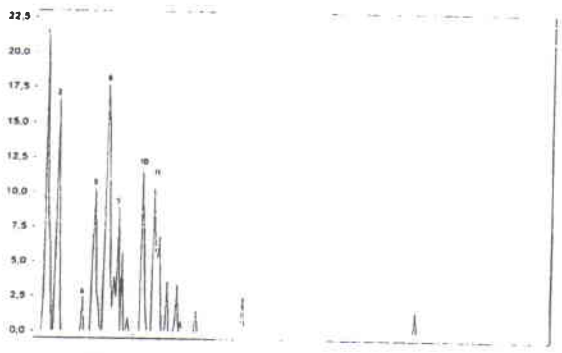

Figure 6b. Measured spectrum of vibration on the test motor with $\alpha_1=120^0$

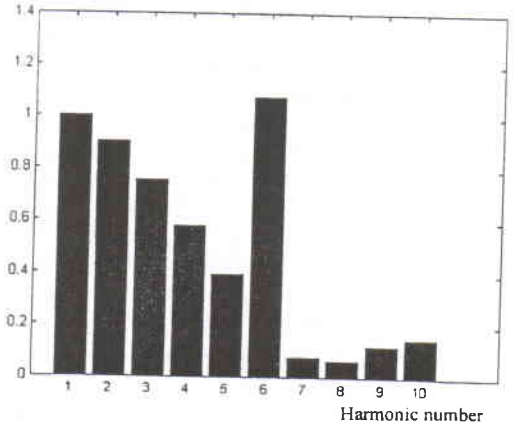

Figure 7. Predicted spectrum of vibration on the test motor with $\alpha_2=150^0$

VI. CONCLUSIONS

A PMDCM has a specific vibration characteristic at no-load depending on the location and size of permanent magnets stuck on the stator. This characteristic provides information about the motor structure and failures. The unbalance MMF created by the magnetic poles can be identified by using the vibration test on the motors. Since this technique also relates the machine dimensions to the spectrum of vibration, the design modification can be done whenever the vibration and noise are important constraints in application, such as wheelchair.

Acknowledgments : We would like to thank Faz Elektrik Co. for founding this work at the Power Electronics and Electrical Machines laboratory at Dokuz Eylül University.

REFERENCES

1] K., J., Binns, P., J., Lawrenson, C., W., Trowbridge, "*The Analytical and Numerical Solution of Electric and Magnetic Fields*", Willey and Sons, 1995.

2] H., A., Toliyat, S., P., Waikar, T., A., Lipo, "Analysis and Simulation of Five-Phase Synchronous Reluctance Machines Including Third Harmonic of Air Gap MMF" *IEEE Transactions on Industry Applications*, Vol. 34, No. 2, March/April 1998, pp. 332-339.

3] S., P., Verna, A., Balan, "Determination of Radial Forces in Relation to Noise and Vibration Problems of Squirrel-Cage Induction Motors", *IEEE Transactions on Energy Conversion*, Vol. 9, No. 2, June 1994, pp. 404-412.

4] S., S., Y., Narayanan, K., R., A., Nair, V., Narayanan, "Design Analysis of Permanent Magnet DC Motors with Differing Armature, Magnet and Yoke Lengths", *IEEE Transactions on Energy Conversion*, Vol. 13, No. 1, March 1998, pp. 55-61.

5] T. Kobayashi, F. Tajima, M. Ito, S. Shibukawa, "Effects of Slot Combination on Acoustic Noise from Induction Machine", *IEEE Transactions on Magnetics*, Vol. 33, no.2, March 1997, pp 2101-2104.

6] R. J. M. Belmans, L. D'hondt, A. J. Vandenput, W. Geysen, "Analysis of the Audible Noise of Three-phase Squirrel-Cage Induction Motors Supplied by Inverters", *IEEE Transactions on IA*, Vol. 23, No.5, Sept 1987, pp 842-847.

7] Philips Handbook on Design of Permanent Magnet Motors.

8] M. G. Say, "*Alternating Current Machines*", Pitman.

9] P. Pillay, "Performance and Design of Permanent Magnet AC Motor Drives" *IEEE -IAS*, tutorial course, 1991.

10] O. Gergöz, "Identification of Noise Source in Wheelchair", M.Sc thesis, DEÜ, September 1998.

11] Functional Description and Operation Application of Vibrometer 20, Schenck.